Aleksandar Grbović[1], Abdussalam Yousef Solob[1], Simon Sedmak[2], Aleksandar Sedmak[1]*

NUMERICAL AND EXPERIMENTAL ANALYSIS OF THE INTEGRITY OF LIGHT AIRCRAFT WING STRUCTURE

NUMERIČKA I EKSPERIMENTALNA ANALIZA INTEGRITETA KRILNE KONSTRUKCIJE LAKE LETELICE

Originalni naučni rad / Original scientific paper
UDK /UDC:

Rad primljen / Paper received: 25.06.2023

Adresa autora / Author's address:
[1)] University of Belgrade, Faculty of Mechanical Engineering, Serbia [*]email: agrbovic@mas.bg.ac.rs
[2)] University of Belgrade, Innovation Centre of the Faculty of Mechanical Engineering, Belgrade, Serbia

Keywords
- stress analysis
- extended finite element method
- wing spar
- CS23 standard

Ključne reči
- analiza naponskog stanja
- proširena metoda konačnih elemenata
- ramenjača
- CS23 standard

Abstract

The wing spar is connected to the supporting elements of the aircraft fuselage through specially designed elements - aircraft fittings. All loads from the wing are transmitted to the main frame and through the wing-fuselage fitting. It is needless to point out the extreme importance of the accurate design of this fitting: its fatigue damage leads to an immediate separation of the wing from the fuselage and a consequent loss of aircraft. During flight, fatigue cracks appear on parts of the wing exposed to tensile stresses. These cracks are monitored, and certain measures are taken when they reach a critical length, but their appearance is not tolerated in the wing-fuselage fittings. This is also the reason why crack growth in these members has not been studied so far and why experimental tests of the remaining fatigue life of the damaged fitting were not required from the manufacturer. Determination of stress state is of great importance as it can be used to predict the locations of potential crack initiation. Experimental and numerical analysis of this problem is presented.

Izvod

Ramenjača je povezana sa nosećim elementima trupa letelice preko posebno dizajniranih elemenata - fitinga za letelice. Opterećenje sa krila se prenosi na glavni noseći ram preko ovih fitinga. Suvišno je ukazivati na izuzetnu važnost preciznog dizajna ovakvih fitinga, pošto pojava zamora u njima može dovesti do trenutnog odvajanja krila od trupa i otkaza letelice. Tokom leta može doći do pojave zamornih prslina na delovima krila izloženim zateznim naponima. Ove prsline se prate i preduzimaju se odgovarajuće mere nakon što dostignu kritičnu dužinu. Međutim, u slučaju veze krilo-trup, njihovo prisustvo nije prihvatljivo ni u kom obliku. Ovo je takođe i razlog zašto rast prslina u njima nije bio predmet istraživanja i zbog čega se od proizvođača obično ne zahteva eksperimentalno ispitivanje preostalog zamornog veka oštećenih fitinga. Određivanje naponskog stanja u ovakvim konstrukcijama i njihovim vezama je od velikog značaja, jer se može primeniti na određivanje kritičnih lokacija u kojima se očekuje pojava prslina. Prikazani su eksperimentalni i numerički pristupi u rešavanju ovog problema.

INTRODUCTION

In order to conduct the fatigue life analysis of the wing-fuselage fitting, it was necessary to determine the appropriate wing loads, Fig. 1. To do that, all necessary aerodynamic parameters were calculated for all load cases /1, 2/ in accordance with EASA CS23 requirements. Based on these aerodynamic parameters the corresponding forces and moments acting on the wing were obtained (including weight of aircraft and fuel), and critical load cases were determined and analysis of the wing structure using finite element method was carried out /3, 4/. The paper focuses on loading cases D023 with following data: m = 920 kg; $W = mg$ = 9022.12 N; n = 6; nW = 54132.71 N; VD = 107.06 m/s; ρ = 1.225 kg/m^3; SW = 15.027 m^2; xWE = 4.486 m; dW = -0.0558 m; dT = 4.4532 m; LW = 57218.20 N; LT = -3085.48 N, as explained in detail, /4/.

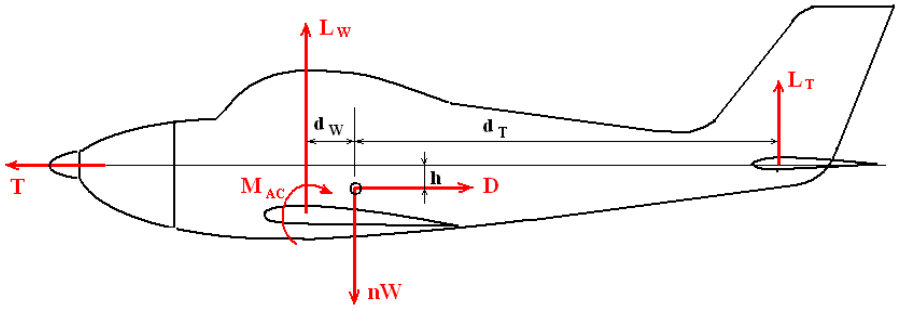

Figure 1. Loads (forces and moments) acting on the aircraft structure.

Wing-fuselage attachment for the light aircraft is shown in Fig. 2. This wing stricture is used in experiments and also as a basis for numerical simulations by finite element method, as shown in /5-12/.

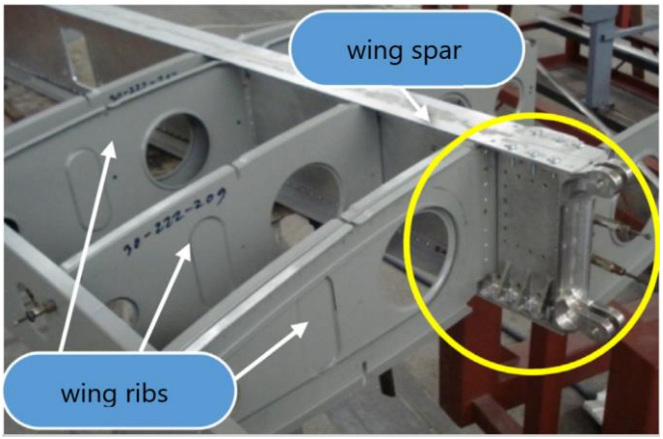

Figure 2. Light aircraft wing-fuselage attachment (circled) with two pairs of lugs, /4/.

WING STRUCTURE ANALYSIS USING FINITE ELEMENT METHOD

For D023 cases the distributed pressure loading is recalculated in equivalent systems of forces distributed along each rib. These forces are distributed over the ribs of the wing. Bending moments at positions of rib cross-sections are equal to moments of distributed pressure loads. The moments of systems of forces and moments of distributed pressure loads on the wing's leading edge are similar too.

Results obtained for transversal forces and bending moments for a case of distributed pressure loads as well as their equivalent concentrated values are shown in Table 1 and presented in more detail in /4/. They are used as input data for the finite element model of wing structure, as shown in Fig. 3.

Table 1. Forces and moments for the D023 case.

Distributed pressure loads				Equivalent concentrated forces	
Y (m)	F_t (N)	M_f (Nm)	F_r (N)	F_{rt} (N)	M_{rf} (Nm)
0	28761.9	62957.566	0	28399.4	62957.566
0.08	28471.8	60685.62	1150.51	28399.4	60685.621
0.337	26696.5	53682.66	1791.9	27248.9	53682.66
0.593	24883.4	47165.68	1943.93	25457	47165.68
0.884	22860.6	40323.38	2213.92	23513	40323.383
1.24	20446.6	32740.896	2346.85	21299.1	32740.896
1.596	18088.3	25993.887	2269.9	18952.3	25993.887
1.922	15960.7	20555.436	2095.28	16682.4	20555.436
2.247	13876.3	15814.63	2046.53	14587.1	15814.63
2.573	11830	11726.408	1990.7	12540.6	11726.408
2.895	9861.32	8329.353	1994.26	10549.9	8329.353
3.23	7880.97	5463.226	1915.81	8555.6	5463.226
3.565	5982.19	3238.893	1814.33	6639.8	3238.893
3.899	4187.69	1627.189	1752.12	4825.46	1627.189
4.235	2512.09	594.546	1243.98	3073.35	594.546
4.56	1055.8	92.727	1829.37	829.369	0

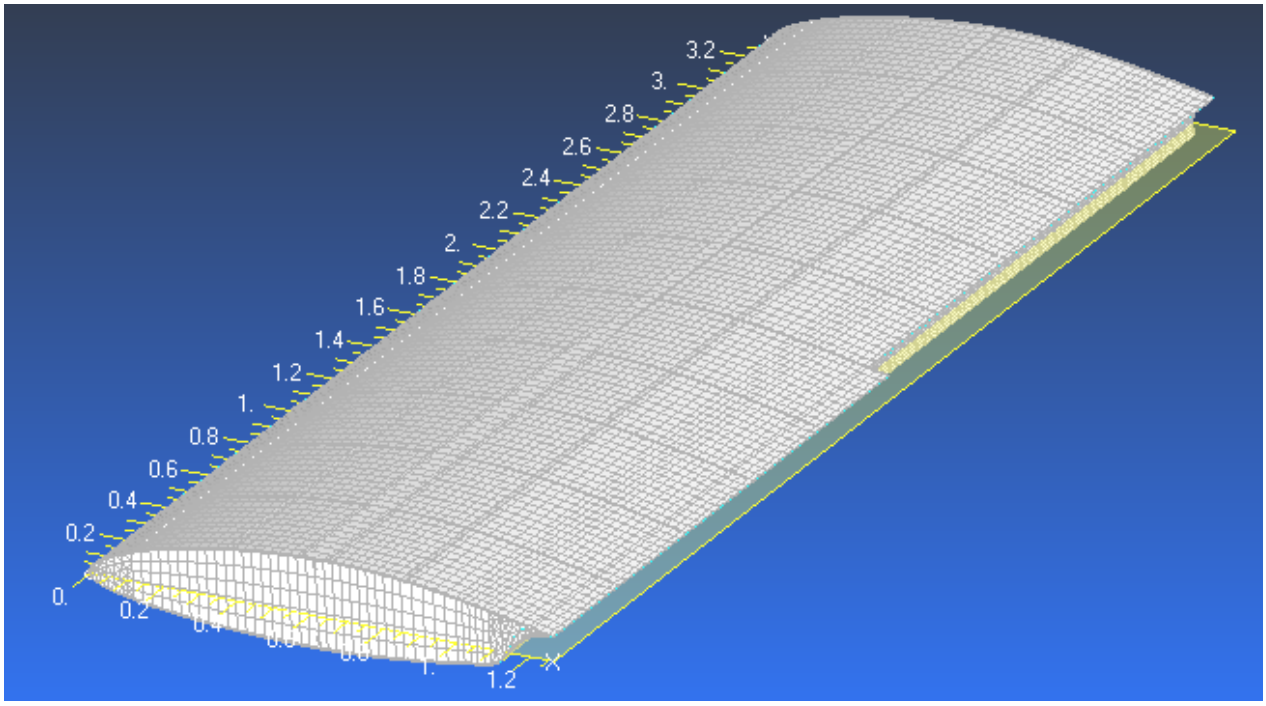

Figure 3. Finite element mesh of the numerical model made in Catia v5.

FINITE ELEMENT ANALYSIS RESULTS

Based on the model briefly presented in the previous section, numerical simulations were performed by using the loads calculated according to the procedure relevant for the D023 case, wherein concentrated forces and moments are defined in corresponding finite element nodes along the wing structure. Results shown in Fig. 4 represent displacements in mm. As expected, maximal displacement occurred at the wing tip. For the load case in question, this displacement was determined to be 98.1 mm.

As can be seen from this example, numerical simulations of wing behaviour (and many other structures) are both efficient and cost-effective, especially when compared to prototype manufacturing and full-scale wing testing. However, the accuracy of the FE model needs to be evaluated and confirmed before a variety of different numerical simulations can be done. Thus, a comparison with experimental values is still necessary, as it is the only way to validate the quality of the numerical model if the deformation of the wing tip obtained in the experiment is close to deformation obtained in FE analysis under the same load. In that case, we can claim that deformations and stresses numerically evaluated in the wing areas not covered in the experiment (e.g. since they are not easily accessible) can be accepted as accurate within a reasonable margin of error.

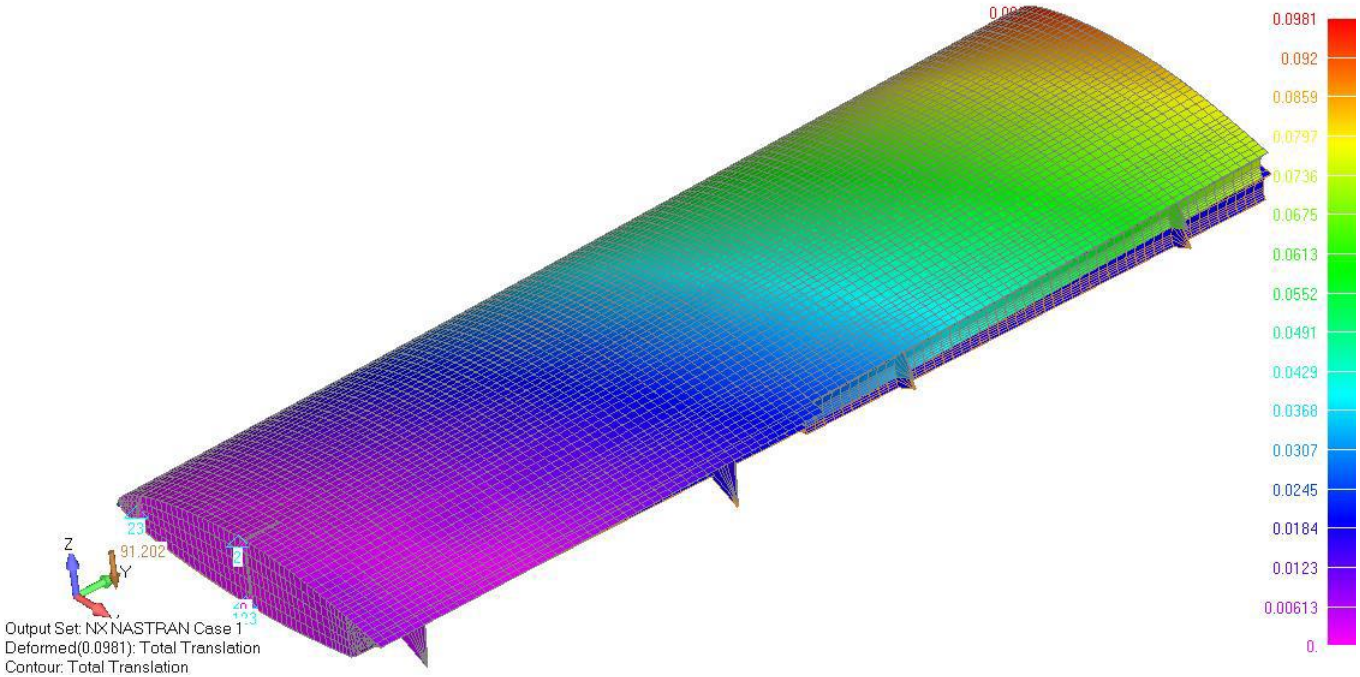

Figure 4. Deformed and undeformed configuration of wing structure for CASE D_0.23 J = 1.55 (maximal displacement at wing tip 98.1 mm).

EXPERIMENTAL VERIFICATION OF NUMERICALLY OBTAINED LOAD

In accordance with the previous conclusions about the necessity of experimental verification for numerical models /13, 14/, a single set of wings (Fig. 5) is manufactured to validate the mechanical behaviour under different loading conditions. The wing prototype used in experiments is shown below.

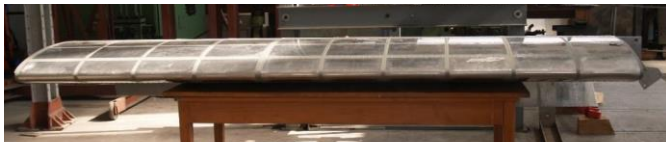

Figure 5. Wing prototype used in the experimental stage.

To measure displacements and strains under predefined loads, a metrology system was installed to correlate the numerical simulation values with test results. As mentioned above, the main goal was to compare the displacements (deflections) measured in different zones of the wing prototype with the ones obtained numerically. Displacements are measured at 10 positions, while the strain is measured at 26 separate locations. In total, 36 strain gauges were glued to the wing on both upper and lower surface (Figs. 6 and 7). The force transducer was also used to measure the applied load. The QuantumX data acquisition system produced by HBM was used. Several 4-channel universal amplifiers were utilised, and collected signals were processed using Catman software from HBM. Catman allows visualization of sensor data, stores data in a binary format, analyses data during the tests, and generates output in different forms (including MS Excel files, an example of which can be seen in Fig. 8).

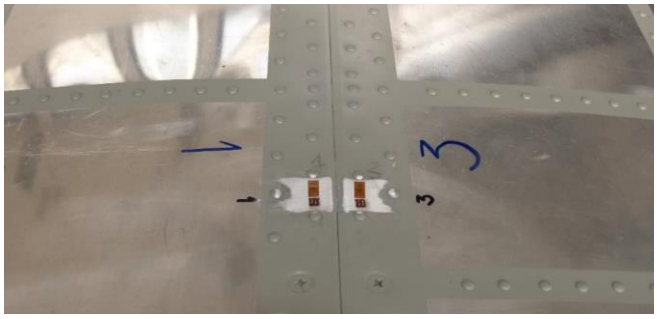

Figure 6. Strain gauges on upper wing surface.

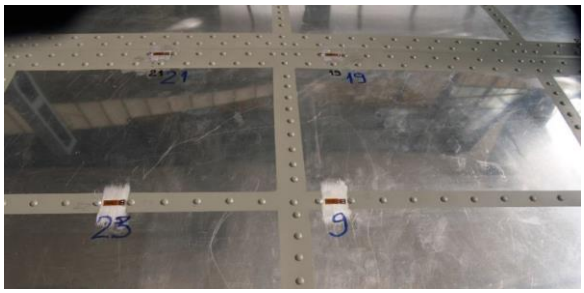

Figure 7. Strain gauges on lower surface of wing.

3	-1	4	1	2	1	3	1	3	1	2
-293	270	-224	107	-26	50	-64	50	-108	95	-53
-611	565	-406	216	-67	66	-170	95	-220	183	-88
-933	808	-600	335	-171	44	-172	147	-417	272	-95
-1074	930	-713	400	-304	-3	-204	170	-478	308	-88
-1196	1030	-804	469	-295	-49	-164	191	-559	343	-68
-1254	1065	-825	502	-283	-75	-122	201	-588	359	-46
-1307	1102	-843	534	-279	-115	-103	209	-615	372	-23
-1354	1146	-859	570	-276	-169	-88	217	-640	386	0
-1390	1169	-865	590	-271	-246	-74	221	-659	392	31
-1393	1167	-866	589	-270	-246	-73	222	-660	393	35
-988	691	-489	287	-247	-171	-146	129	-455	239	-34
-825	524	-372	193	-206	-139	-130	100	-381	185	-49

Figure 8. Example of testing output in the form of an Excel file.

TEST SETUP

The central spar was connected by two pins to a thick steel plate, fixed to the test bench through threaded bolts. This configuration was designed to create infinitely rigid conditions in the wing root, providing conservative test results from the point of view of actual conditions during the flight. More than 20 different loading conditions (cases) were used in wing prototype tests over the period of one month; here, experimental results for the critical loading condition (case D, $n = 6$, no fuel considered) are presented.

The test principle was: once we calculate loads along the wingspan for any case defined by regulations, we introduce them to wing prototype using whiffle-tree /15, 16/. The decision to use a whiffle-tree was made because we needed to apply different loads along the wingspan to simulate the nearly parabolic distribution of aerodynamic forces in combination with inertial forces. Since we had a single hydraulic jack (Fig. 9) to introduce the load, the choice of spreaders and link rods (stirrups) seemed to be the only solution (the alternative approach was to use bags with sand).

Figure 9. Hydraulic jack (with force transducer).

The choice of spreader location allows us to introduce the forces produced by the winglet (the winglet was not attached to the wing during experiments). Stirrup locations and spreader lengths must be determined carefully to impose the load in the experiment that will be close to the load obtained in calculations. It is important that the connecting link rods are normal to the central spar when the load factor reaches 6 g. As a reminder, more than 20 tests were carried out on the test bench and the setting was made to suit all the tests. However, spreader lengths and stirrup positions had to be determined by considering deflections of the wing when the applied load is equivalent to flight conditions with an acceleration of 6 g. The spreaders have been balanced by considering stirrup weight to avoid inducing extra loading to the wing. To protect the wing structure from damage and ensure that the designed load was applied along the wing chord, wooden pads with rubber lining have been used. The wooden pads consist of two separated parts to provide easy assembling and disassembling.

It was decided to apply loads using the whiffle-tree on ribs' positions along the wingspan. As a result, the whiffle-tree shown in Fig. 10 was designed in Catia v5® software, but the determination of stirrup locations and spreader lengths turned out to be a challenging task.

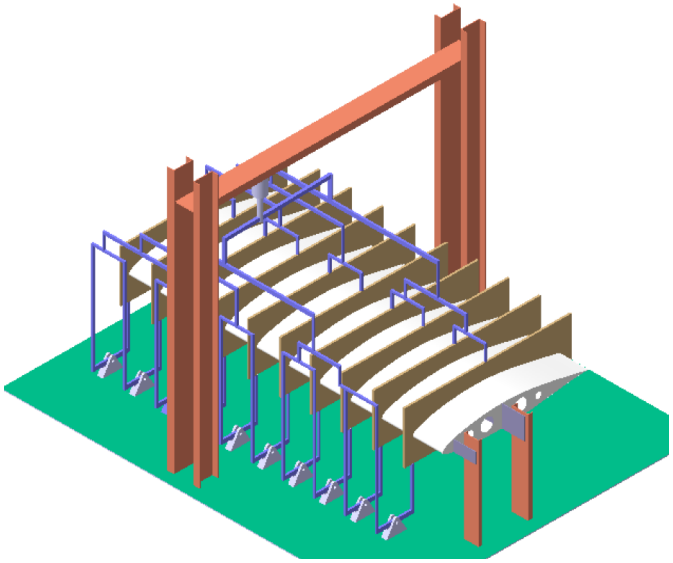

Figure 10. Designed whiffle-tree system for wing structure.

DETERMINATION OF LOADS FOR CRITICAL CASE D AND WHIFFLE-TREE SYSTEM DIMENSIONS

Determining the chord-wise and span-wise distribution of the resultant load, the magnitude of the applied loads, as well as the method of applying those loads on the wing are important steps in the structural test. Here we assume that the *y*-axis goes through the central (main) spar. Calculated loads for this case are given in Table 2.

As mentioned above, the ribs are supported with wooden pads, and through them the loads will be applied. To define the lengths of all stirrups and spreaders as well as their exact positions in whiffle-tree that will provide the application of precise loads on ribs, static equilibrium equations must be used. Forces, moments, and dimensions of the whiffle-tree configuration are shown in Table 3.

Table 2. Calculated loads and moments on ribs.

Rib No.	*y* (m)	LW (N)	Moment (Nm)
1	4.54	706.3	92.6
2	4.206	1669.3	482.4
3	3.872	3474.6	1340.0
4	3.535	5033.1	2729.7
5	3.200	6728.6	4651.3
6	2.865	8517.2	7129.6
7	2.543	10312.0	10053.1
8	2.217	12192.6	13570.2
9	1.891	14125.2	17664.7
10	1.566	15433.4	22337.9

Table 3. Forces and moments for the whiffle-tree configuration.

Rib No.	*y* (m)	Force (N)	Moment (Nm)
1	4.54	300	96
2	4.206	772	454.0
3	3.872	1492	1310.4
4	3.535	1565	2701.9
5	3.200	1608	4623.8
6	2.865	1659	7101.4
7	2.543	1686	10025.8
8	2.217	1906	13607.9
9	1.891	2180	17900.7
10	1.566	2200	22895.3
Total Force (N)		15368	

By comparing the values of moments and forces calculated for the designed whiffle-tree from Table 3 with values in Table 2, it can be seen that the total force of 15368 N that will be introduced by a hydraulic jack is very close to the calculated value of force on the tenth rib 15433.4 N (the eleventh rib is at the position of support, Fig. 11. At the same time, moment 22895.3 Nm on the 10^{th} rib (Table 3) is somewhat greater than the moment 22337.9 Nm (Table 2), but the difference is about 2.5 %. This difference was considered small enough for the model to be acceptable, and the design of the whiffle-tree shown in Fig. 10 was adopted. After that, the test assembly was completed using the manufactured whiffle-tree, as shown in Fig. 12.

Figure 11. The eleventh rib at the position of support.

Figure 12. Test assembly with manufactured whiffle-tree.

WING TEST LOADING AND OBTAINED DISPLACEMENTS AT THE WING TIP

European Aviation Safety Agency's specifications for light aerobatic aircraft define two types of loading that must be applied to the wing structure during testing:

Loading No 1: Load must rise up to the limit load (6 g) in steps, adding 10 % of the load in each step, with a pause of 3 s between steps. Once a 6 g load is achieved, slow unloading is conducted.

Loading No 2: A destructive test is carried out with loading rise until limit load (6 g) as described above, and after, incremental increase of load is applied until wing failure.

Following these instructions, the load introduced by the hydraulic jack was incrementally increased during the test until the maximum force of 15787 N (as measured by force transducer, see Table 4). Since the force was introduced in too many steps, only 15 steps of loading (and unloading) are presented in Table 4.

Table 4. Forces and displacements measured at 10 wing locations.

Force (kN)	S10 (mm)	S11 (mm)
-0.048	-0.171	-0.146
3.557	38.797	40.916
7.002	57.771	59.901
10.493	74.108	75.19
12.272	83.564	84.046
14.027	97.127	98.041
14.921	103.311	103.456
15.787	109.723	109.271
12.426	108.112	109.679
10.483	100.874	103.636
7.522	89.027	93.409
6.796	86.054	90.797
3.492	70.316	76.085
-0.009	36.588	39.371
-0.617	22.245	24.801

Force-displacement diagrams for both S10 and S11 cases (Table 4) are shown in Fig. 13, where it can be seen that the obtained results are very similar, with maximal forces being around 16 kN. Maximal displacements are around 110 mm for both cases, corresponding well with the FEM value of 98.1 mm (Fig. 4).

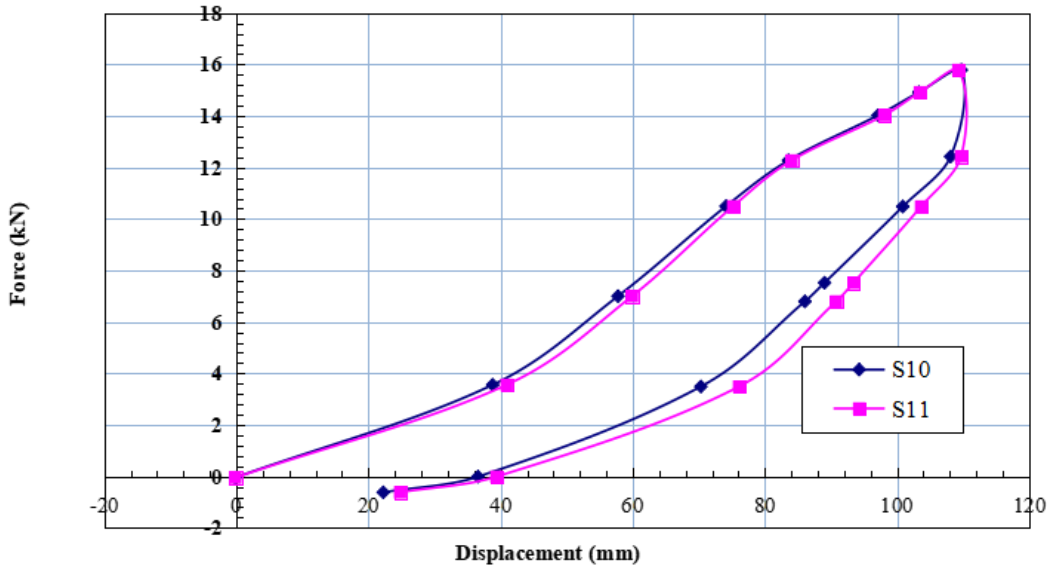

Figure 13. Graph of displacements at the wingtip.

CONCLUSION

The light aircraft wing structure was analysed first, and it was shown that it satisfies strength requirements according to standards CS23. Magnitudes and the distribution of loads have been considered in detail and the distribution of pressure loading was done according to CS23 requirements. The inertial loading was modelled also, and all displacements (translations and rotations) are relatively small which shows that the structure has enough stiffness. A detailed analysis of the state of stresses, deformations, and strength of the wing structure regarding the magnitude of limit loads shows that stresses at structural elements do not exceed the elastic limit. The experimental verification of analytical/numerical results was carried out on the full-scale wing, and it was shown that the difference between deformations was satisfactory low.

REFERENCES

1. https://www.theguardian.com/business/2019/nov/06/boeing-737-cracks-ryanair-grounds-three-planes-due-to-cracking-between-wing-and-fuselage [last accessed 08.14.2023]
2. Barter, S., Sharp, P.K., Clark, G. (1994), *The failure of an F/A-18 trailing edge flap hinge*, Eng. Fail. Anal. 1(4): 255-266. doi: 10.1016/1350-6307(94)90001-9
3. Solob, A.Y., *Fatigue life analysis of damaged light aircraft wing-fuselage fitting*, Ph.D. Thesis, University of Belgrade, Faculty of Mechanical Engineering, 2021.
4. Solob, A., Grbović, A., Božić, Ž., Sedmak, S.A. (2020), *XFEM based analysis of fatigue crack growth in damaged wing-fuselage attachment lug*, Eng. Fail. Anal. 112: 104516. doi: 10.1016/j.engfailanal.2020.104516
5. Sedmak, A. (2018), *Computational fracture mechanics: An overview from early efforts to recent achievements*, Fatigue Fract. Eng. Mater. Struct. 41(12): 2438-2474. doi: 10.1111/ffe.12912
6. Grbović, A., Solob, A.Y., Sedmak, S., Sedmak, A. (2023), *Optimisation of wing-fuselage attachment lug*, Struct. Integ. Life, 23(2): 161-165.
7. Grbović, A., Kastratović, G., Sedmak, A., et al. (2019), *Fatigue crack paths in light aircraft wing spars*, Int. J Fatigue, 123: 96-104. doi: 10.1016/j.ijfatigue.2019.02.013
8. Kara Achira, F.S., Medjdoub, S.M., Hocine, A., et al. (2023), *Numerical analysis of the effect of the repair of corroded pipeline with composite patches on the prediction of failure pressure*, Struct. Integ. Life, 23(1): 15-22.
9. Milovanović, A.M., Martić, I., Trumbulović, Lj., et al. (2021), *Finite element analysis of spherical storage tank stress state*, Struct. Integ. Life, 21(3): 273-278.
10. Radojković, M., Čamagić, I., Šarkočević, Ž., et al. (2021), *Stress distribution on an isotropic plate with a rectangular opening under biaxial tension load*, Struct. Integ. Life, 21(1): 91-94.
11. Medjo, B., Arsić, M., Mladenović, M., et al. (2020), *Influence of defects on limit loads and integrity of the pipeline at hydropower plant 'Pirot'*, Struct. Integ. Life, 20(1): 82-86.
12. Alnagasa, K., Petrović, R., Banaszek, A., et al. (2022), *Stress state analysis of propane butane gas spherical storage tanks*, Struct. Integ. Life, 22(2): 253-256.
13. Aranđelović, M., Petrović, A., Đorđević, B., et al. (2023), *Effects of multiple defects on welded joint behaviour under the uniaxial tensile loading: FEM and experimental approach*, Sustainability, 15(1): 761. doi: 10.3390/su15010761
14. Aranđelović, M., Sedmak, S., Jovičić, R., et al. (2021), *Numerical simulation of welded joint with multiple various defects*, Struct. Integ. Life, 21(1): 103-107.
15. Kim, H.-G., Kim, S., Ha, B.-G. (2022), *Study on the test load for the structural test of the flight-load condition of the external fuel tank for fixed-wing aircraft*, In: Proc. Institution of Mech. Eng., Part G: J Aerosp. Eng. 236(11): 2341-2351. doi: 10.1177/09544100 211062809
16. Kim, H.-G., Kim, S., An, S.-H., et al. (2023), *Validation of the structural integrity of an aircraft external fuel tank through a structural test under flight-load conditions*, Proc. Institution of Mech. Eng., Part G: J Aerosp. Eng. 237(9): 2112-2124. doi: 10.1177/09544100221145790